Middle East Journal of Applied Sciences
Volume: 15 | Issue: 02| April – June | 2025

EISSN: 2706 -7947 ISSN: 2077- 4613
DOI: 10.36632/mejas/2025.15.2.13
Journal homepage: www.curresweb.com
Pages: 150-169

Geotechnical Evaluation of the October- Abu Roash Urban Bedrocks Based on Lithomorphic Analysis of the Volcanic/Clastics Outcrops, Greater Cairo, Egypt

Abubaker I. Abduelgadir, Mohamed A. El-sharkawi, Mohamed I. Elanbawy and Nahla A. Shallaly[1]

Geology Department, Faculty of Science, Cairo University, 12613 Giza Egypt.

Received: 20 April 2025 **Accepted:** 19 June 2025 **Published:** 30 June 2025

ABSTRACT

The October Abu Rawash corridor represents one of the most significant zones of urban expansion in Greater Cairo, having undergone substantial transformation in recent decades due to rapid population growth and associated development pressures. However, this growth has been accompanied by notable geotechnical challenges, primarily stemming from the area's complex and heterogeneous subsurface conditions. The foundation problems are largely attributed to the juxtaposition of clastic soils with highly weathered volcaniclastic bedrock, characterized by abrupt lateral and vertical lithological variations and a dense, multidirectional fracture network. These geological features significantly increase the risk of differential settlement. In addition, the widespread presence of expansive clay minerals both within the volcaniclastic units and the argillaceous Qatrani Sandstone further compromises the mechanical stability of the foundation soils by reducing their bearing capacity and increasing susceptibility to volumetric changes with moisture fluctuations. The region is also exposed to multiple geo-environmental hazards, including slope instability along the main escarpment and rising groundwater levels in the adjacent cultivated urban zones. These hazards are exacerbated by inadequate drainage infrastructure, aging water distribution systems, and seepage effects, particularly in areas underlain by clay-rich volcanic and clastic formations. Moreover, predicted climate change impacts and unsustainable land-use practices may further intensify the associated risks. To address these challenges, a comprehensive geological and geotechnical risk assessment was conducted, incorporating geomorphological, lithological, petrographical, mineralogical, and geoengineering parameters. Based on the integrated analysis, the study proposes a set of targeted management strategies and geotechnical recommendations aimed at enhancing ground stability and supporting future urban development in the area.

Keywords: Settlement, slope instability, geomorphological, lithological, petrographical, mineralogical, and geoengineering parameters

1. Introduction

Globally, land use changes driven by urban expansion have become a prominent focus in sustainable development management, especially in the context of the Greater Cairo cities due to their complex and dynamic growth processes (Arnous *et al.,* 2011; Youssef and Maerz, 2013). The study area represents one of the most rapidly expanding regions within Greater Cairo (see Figure 1). The urban landscape and geo-environmental conditions of Greater Cairo have undergone significant transformation owing to rapid population growth. Furthermore, the area's foundation conditions pose considerable geotechnical challenges, including heterogeneity in soil types such as expansive clays and highly weathered volcanic materials and exposure to geological hazards. Additionally, the region faces ongoing anthropogenic environmental threats, resulting from unregulated urban encroachment on the Nile floodplains and increasing land use pressures, which threaten both the ecological integrity and geological stability of the area.

Corresponding Author: Abubaker I. Abduelgadir, Geology Department, Faculty of Science, Cairo University, 12613 Giza Egypt. E-mail:

Therefore, it is necessary to evaluate the environmental landscape and the geotechnical properties of the foundation bedrocks. This evaluation plays a critical role in understanding the soil and subsurface conditions, which directly influence future land development, infrastructure projects, and urban planning and management.

Accordingly, this study aims to establish guidelines and identify associated lithomorphic features that are recommended as potentially suitable for future urban expansion. This aim can be achieved through the following specific objectives:

1- Geoenvironmental profile and urban change detection.
2- Lithomorphic analysis based on the spatial distribution of landforms and their lithological characteristics.
3- Geological and geotechnical risk assessment based on petrographical, clay mineralogical and geoengineering characteristics.
4- Integrated approach using all collected data to determine and assess the geotechnical characterization of the foundation bedrocks and their expected behavior under changes of land use and climate.

2.The study area

2.1. Physiography

The study area contains the largest urban expansion cities (e.g October, Shaikh Zaied and Abu Roash cities) in Greater Cairo. It is sited in the southwestern sector of the Giza Governorate, within the northern part of the Western Desert. It is nearly defined by latitudes 29^{o} 54'N and 30^{o} 7'N and longitudes 30^{o} 48' 30" E and 31^{o} 7' 30"E encompassing approximately 600km^{2}. The study area is dominated by a hot desert climate with very low annual precipitation and high temperatures throughout the year with high evaporation rates and frequent sandstorms, which are common during the spring and summer months. The area contains a distinct transportation network of roads, railways and monorail (Figure 1). It includes parts of Cairo- Alexandria, Cairo- Fayoom, and ring roads in addition to Marsa Matrouh- Ain Sokhna railway, Daba'a Axis and West Cairo Monorail (Figure 1).

Topographically, the study area has a mostly flat landscape, known as a peneplain, but also includes several hills, plateaus, dry valleys (wadies), and low-lying areas (depressions). Some of the main highland features are the Abu Roash Anticline, El-Hasana Dome, and Qaret Haddadin, which are connected to the Sidr Khamis Depression (Abdel khalek *et.al.,* 1989). The wadies in the area are wide and range from shallow to moderately deep. These wadis have smaller branches (tributaries) that flow toward the cultivated lands and the Nile Valley (Hussien *et al.,* 1987).

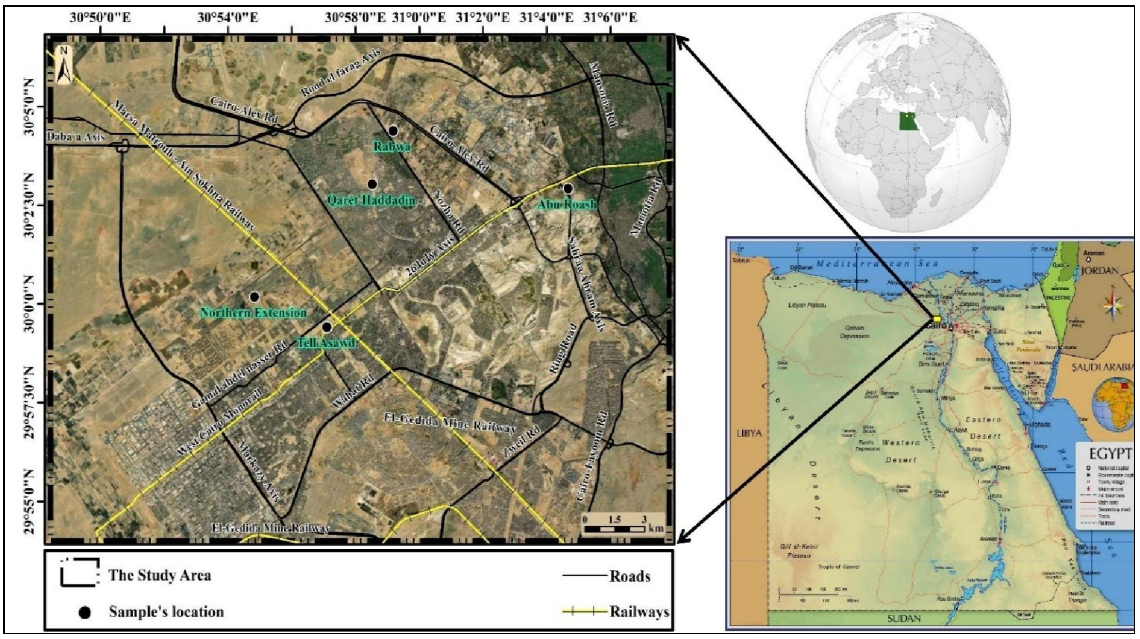

Fig. 1: Location map of the study area showing the study sites, Rabwa, Qaret-Haddadin, Northern Extension, Tell Aswad, and Abu Roash.

The urban areas are built on heterogeneous clayey clastics and weathered volcanic soils, which can cause different types of hazards to buildings, especially with the expected pressure from land use and climate changes. In the future, global changes may increase climate-induced hazards such as flash floods and sandstorms.

2.2. Stratigraphic Setting

The stratigraphic succession of the study area (Conoco geological map, 1987) includes the Cretaceous–Eocene sequence in the El-Hasana Dome (protectorate area, Kuu), surrounded by Oligocene–Miocene clastics of the Qatrani Formation, followed by volcaniclastic–basalt succession, Early Miocene Gebel Khashab Formation, Pliocene, and Quaternary deposits. A brief lithological description of these units is shown in Table (1) and the modified geological map (Figure 2).

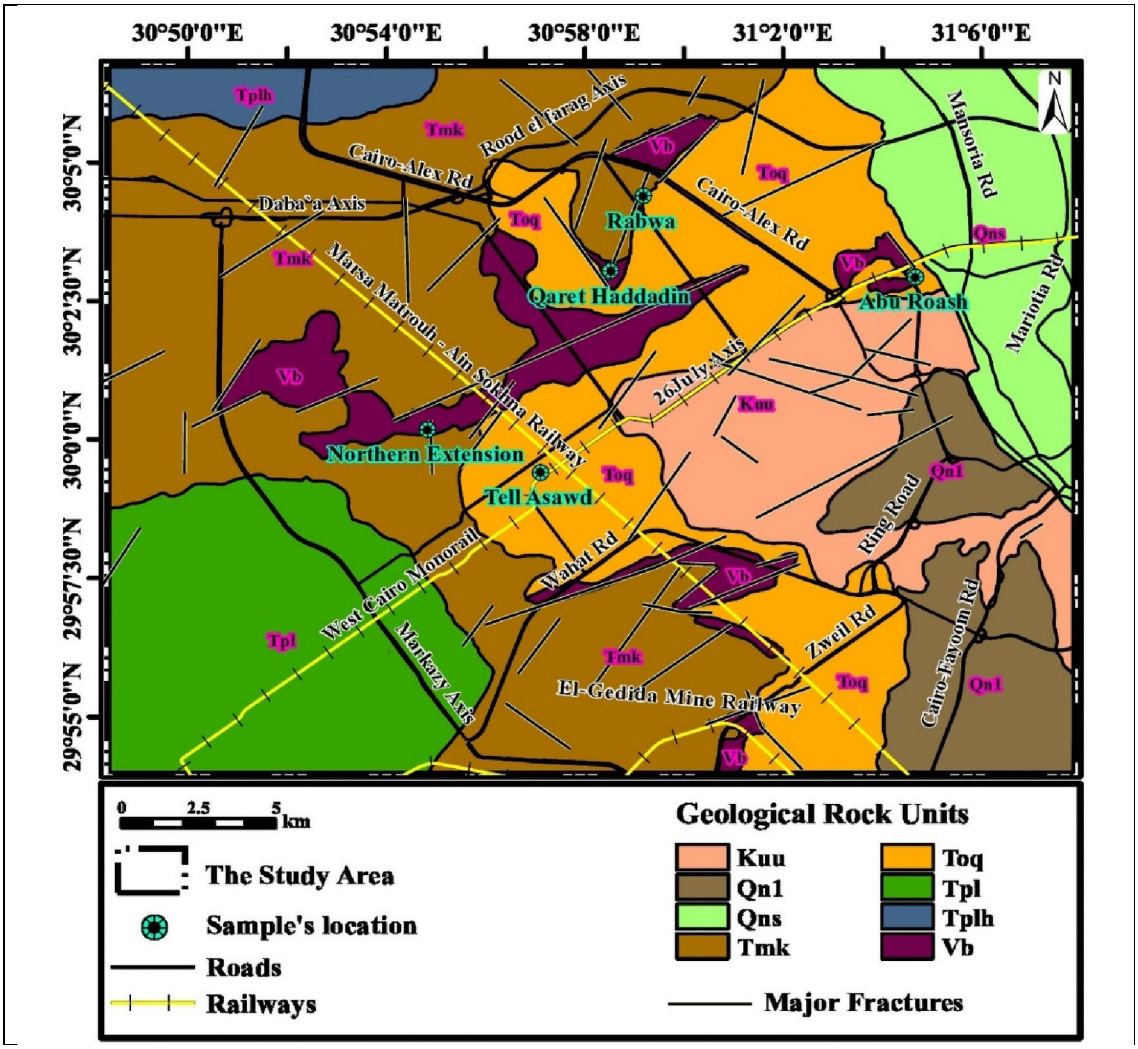

Fig. 2: Geological map of the study area (modified after Conoco 1987), (Kuu): Carbonate (chalk calcarenite), sandstone & siltstone, (Toq): Gebel Qatrani formation, sequence of continental to littoral marine alternating clastics, burrowed siltstone, occasional marine coquina and vertebrate remains. (Vb): Basalt flows and volcaniclastics. (Tmk): Gebel Khashab dark brown continental sandstone locally with petrified wood. (Tplh): El- Hagif formation, white shallow marine limestone with interbedded. (Tpl): Pliocene deposits, undifferentiated. (Qn1): Proto- Nile deposits. (Qns): Cultivate land.

Table 1: Lithological description of the rock units in study area based on the Conoco geological map 1987 (as shown in Figure 2).

Rock units	Brief lithological description
Quaternary Cultivated Land (Qns)	Nile flood mud (Recent)
Proto- Nile deposits (Qn1) (I dfu Formation)	Cobbles and gravels associated with quartz sand grains.
Pliocene deposits (Kom El- Shulal Formation) (TPI)	Paleonile beds consisting of red- brown clays and sand- silt laminae with occasionally shale, calcareous sandstone and limestone interbeds.
El- Hagif Formation (Early Pliocene) (Tplh)	White shallow marine limestone with interbedded marl, sands and bentonitic clays.
Gebel Khashab Formation, Early Miocene (Tmk)	Fluviatile to fluvio- marine red sandstone with marine fauna, occasional silicified woods, and vertebrates.
Basalt flows and volcaniclastic (Vb) (Oligocene)	Several episodes of volcanic activities represented by highly altered volcaniclasic- basaltic layers, massive basalt and layered basaltic flow.
Gebel Qatrani Formation (Oligocene) (Toq)	Fluvitile to littoral marine alternating reddish sandstone and mudrocks with occasional marine coquina and vertebrate remains.
Eocene- Cretaceous limestone and clastics sequence (Kuu)	Marine to fluviomarine limestone, chalk and calcareous sandstone, showing fracturing and karst features.

3.Methodology

3.1. Desk work

Mapping of geomorphic features, topographic contours, and environmental changes was done using a 30 m resolution DEM, L-band PALSAR data, and Esri Bing maps. GIS and RS techniques, supported by field investigation, were used for lithomorphic analysis and mapping of hazards and urban change. Band combination, band ratio, and supervised classification of Landsat-8 data from 2000, 2010, and 2020 were used to study urban expansion.

3.2. Field work

The field work was important not only for describing the stratigraphic sections and collecting representative bedrock samples, but also for checking the data from previous geological maps and remote sensing results, as it gives ground-truth information. It also helps in understanding the local environmental profiles and the factors controlling geo-hazards and anthropogenic factors.

3.3. Laboratory analysis

Laboratory analysis included petrographical and mineralogical investigation of compacted and friable bedrock samples. Selected samples were studied petrographically at Cairo University using thin section microscopy. Some were also analyzed by X-ray diffraction (XRD) at the Tebein Center in Helwan.

Both powdered bulk samples and separated clay fraction (> 2µm) were X-rayed using XRD (Bruker Co. D8 Discover, Germany) with a Cu target, 1.054 Å wavelength, Ni filter, 40 kV, and 40 mA.

Clay minerals were identified from XRD charts of untreated, glycolated, and heated (550 °C for 2 hours) oriented clay fraction slides. Minerals in both bulk samples and clay fractions were identified using ASTM cards and standard references. Their relative abundance was semi-quantitatively estimated using the peak areas of their characteristic lines.

3.4. Geotechnical tests

Geotechnical information for the compacted bedrocks includes compressive strength (CS), Los Angeles abrasion, absorption, and degradation tests. For the friable bedrocks, it includes mechanical analysis, moisture content (WC), California Bearing Ratio (CBR), and modified Proctor (MP) tests.

Compressive strength is the ability of a material to withstand loads, and its ultimate value is the uniaxial compressive stress at complete failure. It is measured through a compressive test by applying a uniaxial load until the material breaks. The Los Angeles Abrasion Value shows the percentage of wear in aggregates due to rubbing with steel balls and is tested according to Aashto, (2002).

Water absorption is used to measure the amount of water a material takes in. The test is carried out according to ASTM-D570 (1998).

Degradation in engineering refers to the damage that occurs to materials or machines due to constant, repetitive stress from natural or anthropogenic processes, which can reduce their mechanical or physical properties.

Mechanical analysis determines the grain size of friable material as a percentage of total dry weight, using sieve analysis (dry) and hydrometer analysis (wet). Water (moisture) content is the ratio of pore water mass to the mass of soil solids, tested according to ASTM-D2216 (2019). The California Bearing Ratio (CBR) test evaluates soil suitability for sub-grade and subbase layers, following ASTM-D1883 (2021). The Proctor Compaction (PC) test is used to find the maximum dry unit weight and optimum moisture content, following ASTM D1556-07 (2007).

4. Result and Discussion

4.1. Lithomorphic characterization

Several factors influence the development of bedrocks and soils to be suitable for foundations, including topographical slope, hardness and uniformity, structural types and intensity, as well as hydrological and climatic conditions. Surface erosion, which shapes the current landforms, is also controlled by these factors. To study the effects of geological and hydrological factors on bedrock and landform development, the area is divided into high relief landforms (e.g., P, H, C, and D) and low relief landforms (e.g., W, T, and F) as shown in Figure (3).

The escarpmental plateau (P), with an altitude above 192 m a.s.l., is the largest highland in the central southern part of the area (Figure 3). To the northwest, it gradually merges into the rocky talus cover (C) at 144–192 m a.s.l. This talus also appears around the plateau with varying slope angles and near the edges of the volcanic-clastic isolated hills (H). The spaces between landforms P, H, and C are filled by wadi plains and wadi channels (W).

The entire plateau (P) is locally divided into fault blocks by several fault trends (e.g., E–W, N–S, NW–SE, and NNE–SSW). The linear escarpment edges align with major faults trending NNW–SSE. The central plateau (P), formed mainly by Gebel Qatrani and Gebel Khashab formations (Fig. 2), has a mostly flat top with steep, irregular eastern fault escarpments (Fig. 3), which are prone to instability hazards. A faint drainage pattern occasionally dissects the plateau surface.

Several volcanic exposures appear in irregular forms of volcaniclastic and basaltic sheets, flows, and hills (H), such as in Qaret El-Haddadin, Rabwa, Northern Extension, Tell Aswad, and Abu Roash (Fig. 3). These exposures are mainly concentrated in the northwest part of the area and extend a few kilometers along NE–SW and NW–SE fault trends within the gently sloped basaltic-sandy talus cover (C), likely derived from nearby plateaus and hills. Scattered volcanic exposures also appear along the eastern escarpment of the central plateau (P). Typical domal volcanic-clastic hills like Qaret Haddadin and Tell Aswad show volcanic layers between the Qatrani Sandstone below and Khashab Sandstone above. Other exposures, such as in Abu Roash, show volcanic-clastic units topped by basalt sheets over the Qatrani Formation (Fig. 3).

The last high relief landform is the Al Hassana Dome–ridges, located south of the Abu Roash area near the Cairo–Alexandria Road (Figure 3). It consists of a circular anticlinal domal plateau with associated structural ridges. The dome is bounded to the north by a major fault escarpment trending WNW–ESE. Several circular and non-circular ridges (cuestas) appear to the southeast, mainly trending NE–SW (Figure 3). This structural landform is made up of highly fractured Cretaceous–Eocene carbonate–mudrock beds.

The most important and widespread low relief unit is the desert wadi plains (W), located between the higher landforms like plateaus, hills, and talus cover (Fig. 3). These plains are partly covered by movable sand in the form of patches, mounds, and sheets, and are dissected by shallow wadi channels. Like other Western Desert wadis (Embabi, 2004), these channels form a paleodrainage system likely developed along faults during the Pleistocene pluvial period and are now mostly abandoned due to aridity. Wadi basins formed in areas of intense erosion under structural and lithological control. A water divide along the plateau and hilltops separates them into western and eastern basins. The eastern basins are more linear and drain toward the Nile terraces (T) and flood plain (F), while the western ones drain into the internal low desert areas (Fig. 3).Stratigraphically, the area includes the lower G. Qatrani clastics of Oligocene age, overlain by three basaltic flows (B1–B3), and then by the Miocene G.

Khashab Formation (Fig., Shallaly, 1998). This Tertiary sequence is faulted against Cretaceous limestones along the Cairo–Alexandria Road.

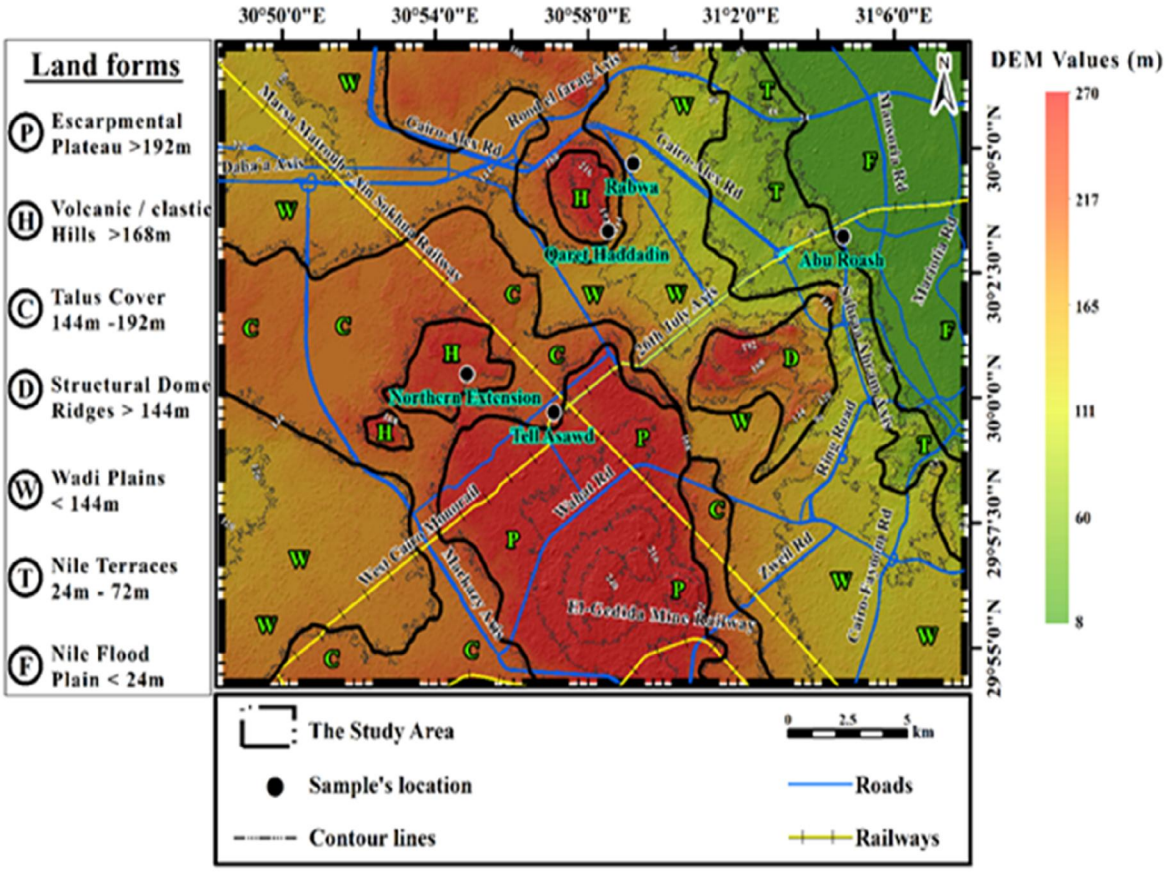

Fig. 3: Landforms of the study area: (P) Plateaus (more than 192m), (H) Volcanic-Clastic Hills (>168m), (C) Talus Cover (144-192m), (W) Wadi Plain (<144m), (T) Nile Terraces (72-24m), (F) Nile Flood Plain (<24m) and (D) Structural Dome- Ridges (>144m*).*

4.2. Urban expansion pattern

To document urban expansion over time in the October–Abu Roash area, it is useful to divide the region into urban units based on physiographical and lithomorphical features. The area is divided into eleven litho-physiographic urban units, numbered 1 to 11 as listed in Table 2. Their spatial distribution over different lithologies, as shown in the geological map (Figure 2), is illustrated in Figure 4. Most exposed bedrocks in these units are dominated by clastics, while units 1, 2, 3, and 4 also include volcanic bedrocks (Table 2).

Change detection analysis of urban expansion in the October–Abu Roash area is based on satellite images from 2000, 2010, and 2020 (Figure 5). In 2000, urban areas expanded progressively at the expense of Nile floodplain cultivated lands and surrounding terraces, especially in urban units 11, 1, and 9. Between 2000 and 2010, rapid urban growth extended toward the October desert region along the 26 July Axis, West Cairo Monorail road, and Wahat road. From 2010 to 2020, urban areas grew significantly in plateau and hill landforms (e.g., units 4 and 7), followed later by units 2 and 6. Most urban development is concentrated near main roads in desert areas and along the river, often filling vacant land within already developed areas.

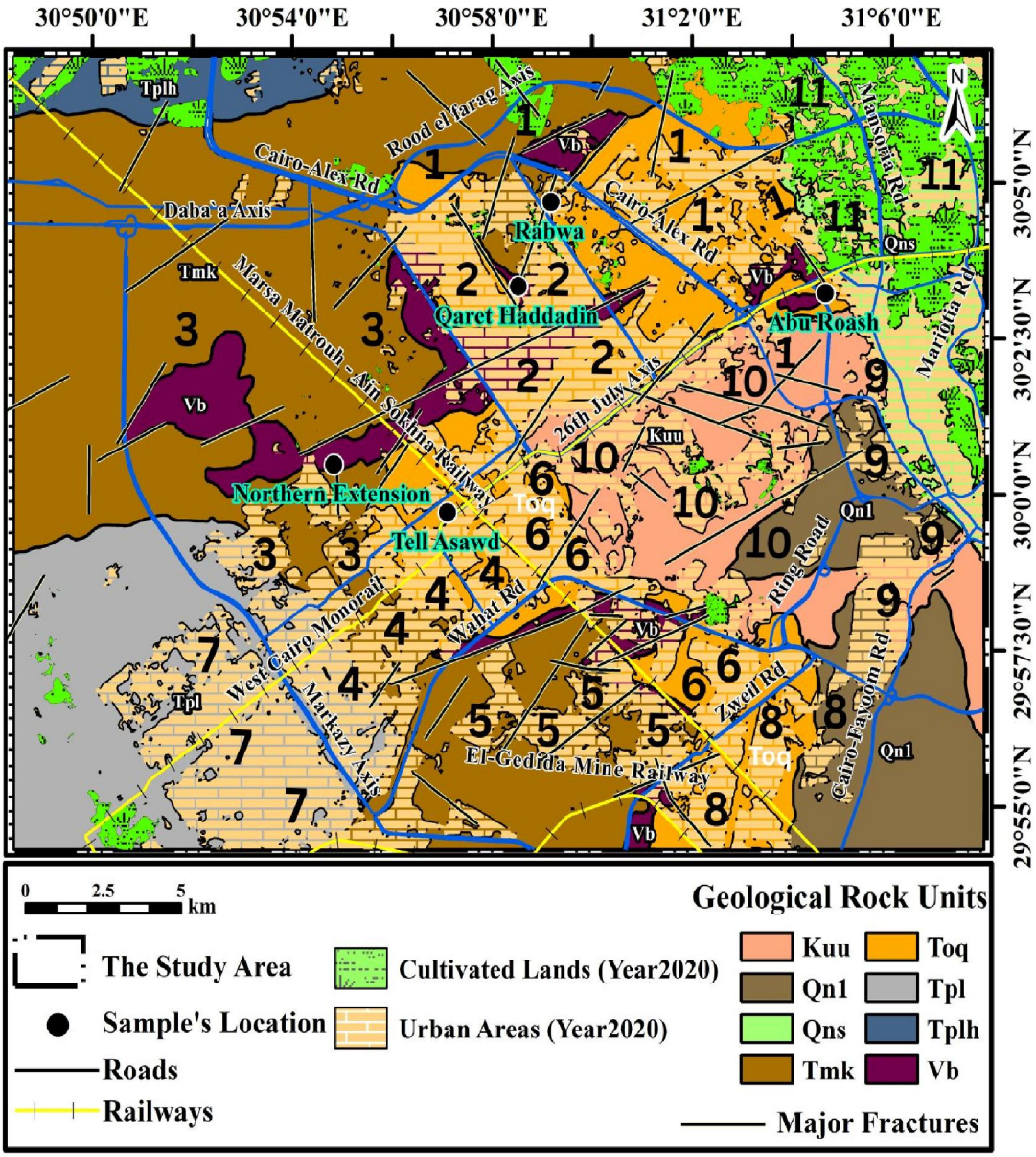

Fig. 4: Physiographic urban units (units No 1- 11) based upon the geological rock units (modified after Conoco 1987), (Kuu): Carbonate (chalk calcearenite), sandstone & siltstone, (Toq): Gebel Qatrani Formation, sequence of continental to littoral marine alternating clastics, burrowed siltstone, occasional marine coquina and vertebrate remains. (Vb): Basalt flows and volcaniclastics. (Tmk): Gebel Khashab dark brown continental sandstone locally with petrified wood. (Tplh): El- Hagif Formation, white shallow marine limestone with interbeds. (Tpl): Pliocene deposits, undifferentiated. (Qn1): Proto- Nile deposits. (Qns): Cultivate land.

In conclusion, from 2000 to 2020, the 600 km² study area experienced major land use changes. In 2000, desert covered 88.50% of the land, with agriculture at 10.18% and urban areas at just 1.32%. By 2010, desert land decreased to 77.95%, agriculture to 8.13%, and urban areas increased to 13.92%, marking the start of urban growth. The most significant shift occurred by 2020: desert land dropped to 54.20%, urban areas rose sharply to 39.19%, and agriculture declined further to 6.61%. These changes reflect a strong shift from natural desert to urban development, driven by population growth, urban sprawl, and development pressures, while agricultural land continues to decline (Figure 5).

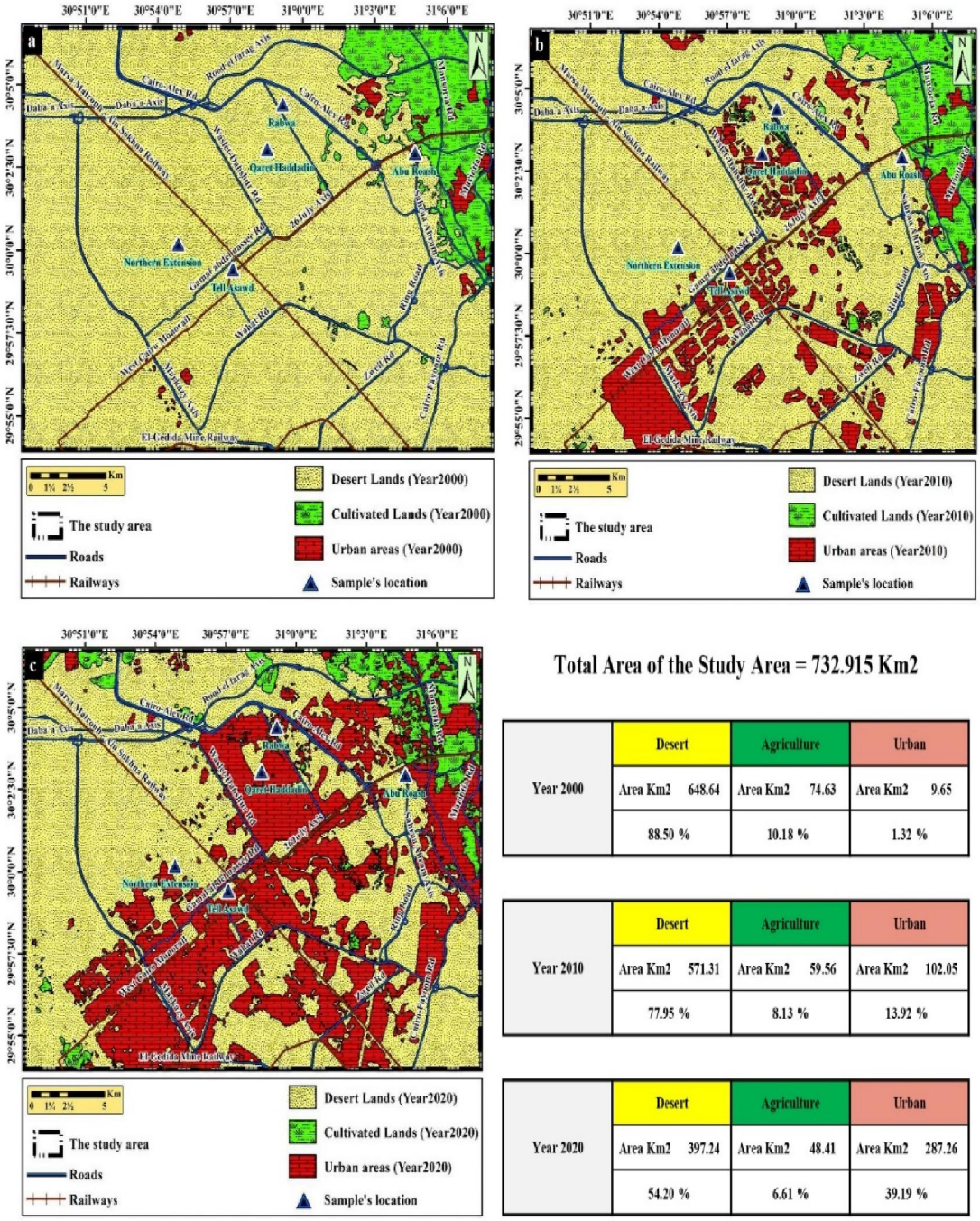

Total Area of the Study Area = 732.915 Km2

	Desert	Agriculture	Urban
Year 2000	Area Km2 648.64	Area Km2 74.63	Area Km2 9.65
	88.50 %	10.18 %	1.32 %

	Desert	Agriculture	Urban
Year 2010	Area Km2 571.31	Area Km2 59.56	Area Km2 102.05
	77.95 %	8.13 %	13.92 %

	Desert	Agriculture	Urban
Year 2020	Area Km2 397.24	Area Km2 48.41	Area Km2 287.26
	54.20 %	6.61 %	39.19 %

Fig. 5: Urban expansion change detection from 2000, 2010 and 2020 of the study area.

Table 2: Locations of the physographic urban units (1-11 inclusive) and their bedrock lithologies based on figure 4.

Units No. (Fig. 4)	Units localities nearest roads (Rd) & other means.	Main lithology of exposed bedrocks			
		Volcanics	Sandstone & Muddy clastics	Limestone	Nile Silt
1	Abu Roash unit (Cairo-Alex-Rd)	(✔)	(✔)	(_)	(_)
2	Rabwa- Haddadin Unit (Waslet - Dahshur Rd)	(✔)	(✔)	(_)	(_)
3	Northren Extension Unit (Marsa Matrouh Rail way Rd)	(✔)	(✔)	(_)	(_)
4	Tell Aswad (Wahat Rd & Abdel Nasser Rd)	(✔)	(✔)	(_)	(_)
5	El–Hadaba (El- Gedida Mine Railway)	(*)	(✔)	(_)	(_)
6	El- Hadaba Sharq (Zwell Rd)	(*)	✔	(_)	(_)
7	El-Hadaba Gharb (West Cairo monorail Rd)	(_)	✔	(_)	_
8	El- Hadaba Ganob (Cairo- Fayoum Rd)	(_)	✔	(_)	(_)
9	El- Hassana Sharq (Sahrraa Ahram Axis)	(_)	✔	(_)	(_)
10	El- Hassana Dome (Ring Rd)	(_)	(✔)	(✔)	(_)
11	El- Mariotia- Mansoria Rd	(_)	(_)	(_)	(✔)
(✔) exposed		(_) not exposed		(*) few scattered exposures	

4.3. Geotechnical Characterization

4.3.1. Petrography of the bedrock

The bedrocks consist of two major lithotypes: basalts (B3 and B2 after Shallay, 1998) and sandstones. Both units show lateral and vertical facies variation (Fig. 6a). The sandstones that belong to the Qatrani Formation are vari-colored and vary in thickness from a few meters to about 30 m. Stratigraphically, these sandstones start with a lower reddish ferrugineous unit, overlain by a pinkish silty sand unit, topped by a greenish white sandy unit (Fig. 6a). Though the basaltic rocks mainly overlie the greenish white sandstone, they may also top the other units depending on the paleotopography during the eruption of the basalts. The basaltic rocks that may reach 10m thick comprise a lower pyroclastic unit best recorded in Rabwa and Northern Extension. It is topped and frequently mixed with a highly altered glassy basaltic B3 flow (Fig. 6b), and the base of the flow is sometimes mixed with sandstone to form an irregular thin horizon of pepreite. This horizon reflects the synchronous volcanism and deposition of sediments in an aqueous environment. The uppermost B2 flow in the area is a massive black basaltic flow with ill-defined columnar jointing. The base of this flow is slightly altered and sometimes juxtaposed along normal faults with the lower flow (Fig. 6c).

A- Basalt bedrock (B2)

Microscopically, this rock is a slightly altered holocrystalline porphyritic olivine basalt. It comprises subhedral to anhedral prismatic, frequently twinned, and zoned plagioclase phenocrysts. Augite appears as fractured glomerophenocrysts, sometimes ophitically enclosing plagioclase. Olivine is locally altered to brownish-yellow smectite, rimmed by reddish-brown iddingsite.

Smectite fills fractures within the groundmass and microfractures that cut across other minerals (Fig. 6d) The groundmass consists of fine plagioclase laths and augite crystals, showing an intergranular to subophitic texture and alteration at the base of the flow to a mixture of smectite, carbonate, and sericite after olivine, augite, and plagioclase (Fig. 6e).

As revealed by the XRD chart (Figure 8a), the plagioclase crystals are mainly labradorite, while the dolomite is predominantly of the ankerite variety (Table 3).

B- Volcaniclastic bedrocks

These types of bedrocks, with their different varieties pyroclastic, lava flow, and pepperite, are spatially distributed in urban units (1), (2), (3), and (4).

Highly altered amygdaloidal basaltic rock

This rock represnts the central part of the lower flow B3. Microscopically, it consists of plagioclase, carbonates, and opaques scattered within a glassy groundmass. The alteration is severe, with original basaltic minerals largely replaced by carbonates, iron oxides or hydroxides, and clay minerals (Fig. 6f). The pagioclase occurs in two generations: large subhedral, fractured, twinned, and zoned tabular crystals, and small, highly sericitized, twinned prismatic crystals forming the main part of the hypocrystalline groundmass. They show an intersertal texture, with smectite and calcite filling the spaces between them. Glassy mesostasis is locally present with acicular iron oxides in the groundmass. No fresh pyroxene or olivine is observed; both are fully calcitized. Amygdules of various sizes contain fibrous zeolites at the rims, followed by smectite, with dolomite and calcite in the cores (Fig. 6g).Although zeolite minerals were not detected by XRD analysis, this is likely due to their small quantity. The XRD data (Figure 7b) show a high content of feldspars, followed by dolomite (ankerite), calcite, and halite (Table 3).

Tachylitic scoriaceous basaltic rock

This unit represents the upper and lower margins of the B3 flow. Petrographically, the lava flow samples are scoriaceous basalt with over 25% vesicles by volume (Fig. 6h). The rock is hypohyalline, with more than 40% mesostasis made up of randomly oriented plagioclase microlites in a black tachylytic glassy matrix. The tachylite shows varying degrees of palagonitization, forming a brownish-orange palagonite gel due to hydration (Fig. 6i). Large euhedral to subhedral, often fractured plagioclase phenocrysts/microphenocrysts are present, slightly altered to sericite and sometimes corroded by the glass. Brown prismatic patches of calcite, smectite, and iddingsite pseudomorphsof olivine and pyroxene.

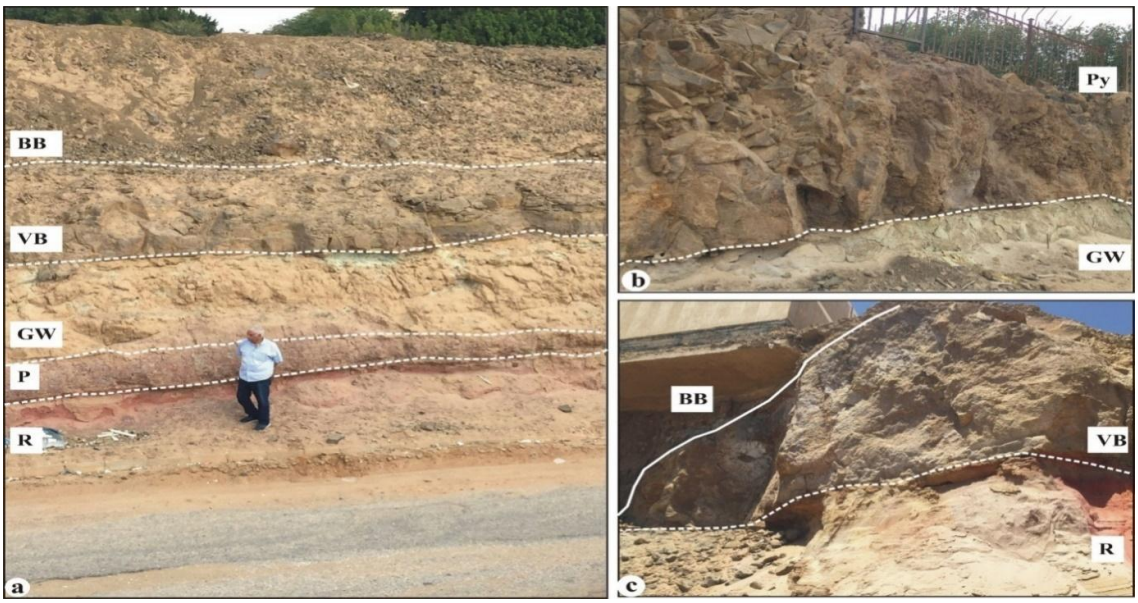

Fig. 6:a-c field photos of the studiedv outcrop: a) Stratigraphy of the area showing a clastic sequence of the Qatrani Fm. Overlain by the basaltic rocks, R: red, P: pink, GW: greenish white, VB: volcaniclastic bedrock, BB: basalt bedrock. Rabwa, looking N. b) A greenish white silty sandstone overlain by a pyroclastic unit, Rabwa, looking E. c) Ferrugineous sandstone (R) overlain by volcaniclastic bedrock(VB) juxtaposed along fault with the basaltic bedrock (BB). Qaret El Haddadin, looking NE.

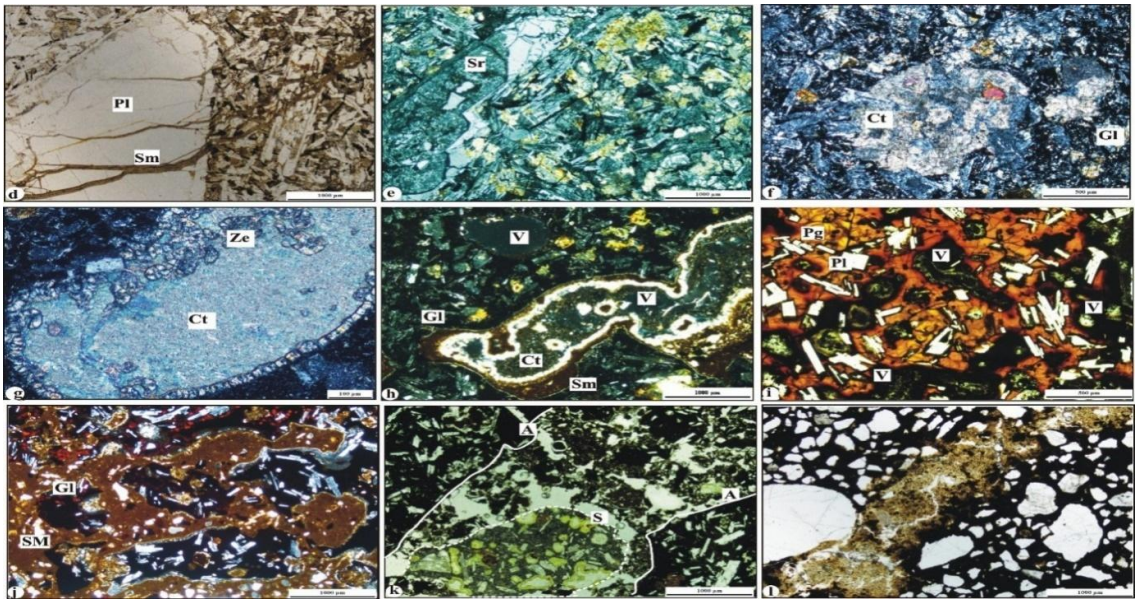

Fig. 6 Cont.: d: l Microphotographs of the studied rocks:d) A large and fractured plagioclase (Pl) phenocryst with brown smectite (Sm) filling the fractures, PPl. e) Highly sericitized plagioclase (Sr), with altered ferromagnesian minerals, CN. f) A large calcitized (Ct) pyroxene with sericitized plagioclase laths in a glassy mesostasis, CN.g) An elongated amygdale filled with calcite (Ct) and rimmed by zeolite (Ze), CN. h) Scoriaceous basalt with irregular vesicles to rounded (V) filled with calcite and rimmed by smectite, within glassy mesostasis (Gl), CN. i) Orange palagonite (Pg) with dispersed plagioclase (Pl) and variably-sized vesicles (V), PPl. j) A peperite with glassy basaltic clasts (Gl) mixed with sandy mud (SM), CN. k) Juvenile scoriaceous (S) and amygdaloida (A) basaltic clasts in a tufaceous matrix of the pyroclastic unit, PPl. l) A ferruginous, poorly sorted sandstone, PPl.

These secondary minerals also fill veinlets and amygdules, showing inward palagonite zoning, followed by smectite, calcite, and iron oxide in the core. At the base of this flow, clasts of the glassy basalt are intermingled with sandy mud, forming pepperites (Fig. 6j). Highly altered plagioclase laths are embedded in the black glass, which shows partial devitrification along its rims to palagonite. The muddy sand contains anhedral quartz grains of fine sand size (Fig. 6j).
The most abundant minerals, as revealed by the XRD chart (Figure 7d), are calcite and dolomite (ankerite), followed by quartz, feldspars, halite, gypsum, and anhydrite (Table 3).

Pyroclastic rock

This pyroclastic rock consists of large, rounded juvenile and accidental lithic clasts surrounded by tuffaceous material. The juvenile clasts are bomb to lapilli-sized, flattened, and of two types: scoriaceous glassy and amygdaloidal glassy basalts (Fig. 6k). The scoriaceous glassy basalt is less abundant. It comprises plagioclase and highly altered ferromagnesian microphenocrysts embedded in a glassy mesostasis. The latter exhibits variolitic texture with radiating plagioclase microlites, numerous, rounded to irregular vesicles are rimmed by yellow smectite and cored by calcite (Fig. 6k). The amygdaloidal glassy basalt is composed of black glassy matrix with few rounded brown amygdules. Randomly oriented, variably-sized euhedral, equant to prismatic twinned plagioclase laths are dispersed in the matrix. The accidental lithic fragments are poorly sorted, subangular to subrounded, and range from coarse to medium sand-size lithic arenite. They comprise monocrystalline to polycrystalline quartz and, less commonly, feldspar grains. Vugs between clasts are irregular to elongated and filled with palagonite, smectite, and dolomite–calcite crystals. The XRD chart (Fig. 7c) and Table 3 show that carbonate minerals, feldspar, and smectite dominate the rock.

C- Sandstone bedrocks

The sandstone of the Qatrani Formation represents the majority of the bedrocks across all urban units. Various types are recorded, including ferruginous, argillaceous, dolomitic, and fossiliferous

sandstones (Fig. 6l and m). It is a moderately to poorly sorted, coarse to medium, subangular to subrounded sandstone. It consists mainly of monocrystalline and less commonly, polycrystalline quartz grains, with some plagioclase and K-feldspar in a clayey matrix. The rock is cemented by calcareous minerals, with colorless calcite rims surrounding brown dolomite rhombs at the cores.
The XRD chart reveals that the dominant mineral is quartz, followed by feldspars, goethite, and dolomite (Figure 7e and Table 3).

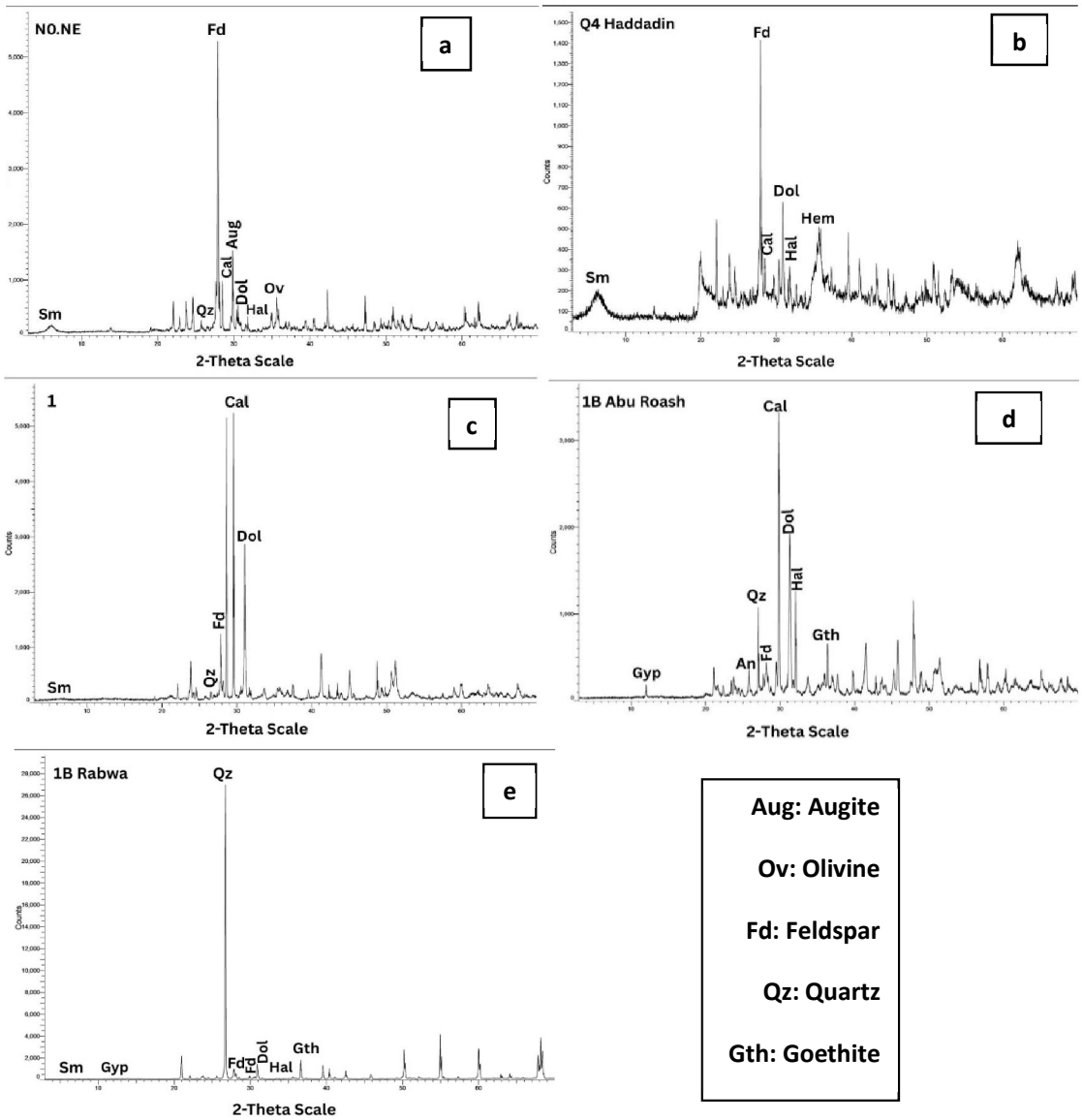

Fig. (7a,b,c,d,e): XRD bulk samples, a. N0 Northren Extension, b.Q4 Haddadin, c. 1, d.1B Abu Roash, e. 1B Rabwa.

Clay mineral identification

X-ray diffraction (XRD) analysis indicates that two types of smectite Ca-montmorillonite and Na-montmorillonite are identified in the separated oriented clay fractions of the studied bedrocks.

Ca-montmorillonite is identified by d-spacings of 15.0–14.8 Å in the clay fraction of slightly altered basalt and volcaniclastic bedrocks in urban units 3 and 2. Na-montmorillonite is identified by d-spacings of 12.78 Å and 12.30 Å in the Rabwa Qatrani Sandstones.

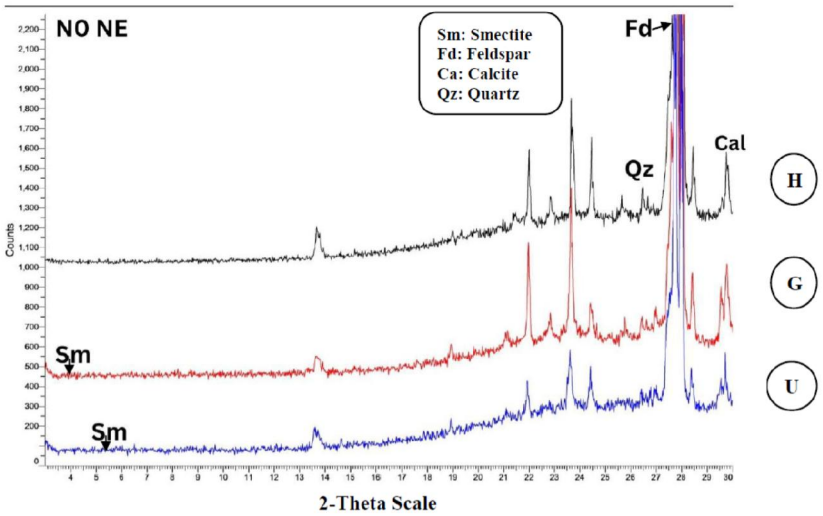

Fig. 8a: XRD chart of the oriented clay fraction of slightly altered basalt sample (N0), north extension (urban units 3&4) (U), (G) & (H) represent untreated, glycolated & heated clay fractions respectively.

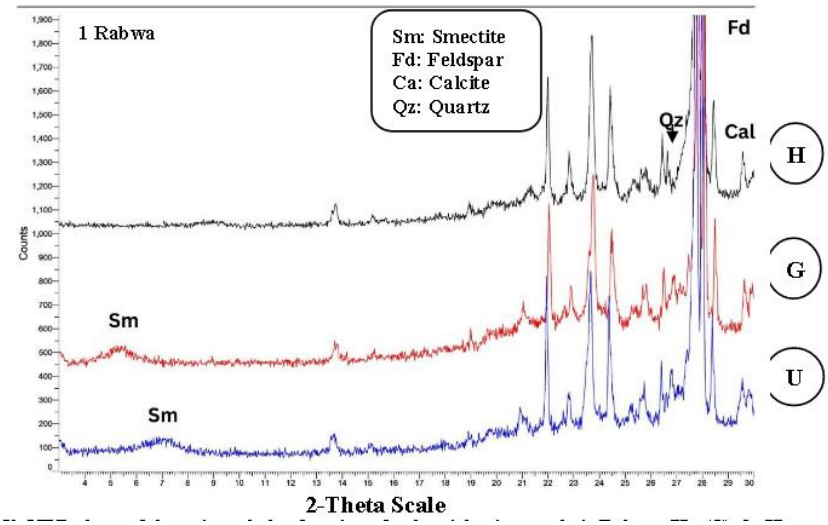

Fig. 8b: XRD chart of the oriented clay fraction of volcaniclastic sample 1, Rabwa (U), (G) & (H) represent untreated, glycolated & heated clay fraction respectively.

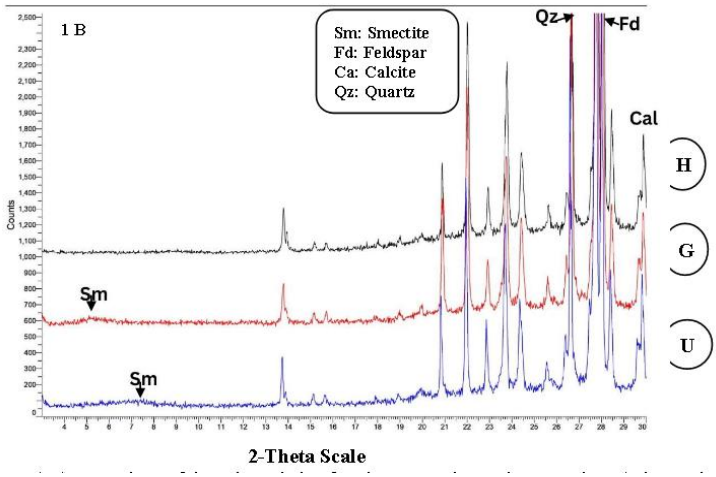

Fig. 8c: XRD chart of the oriented clay fraction Qatrani sample 1B, Rabwa (urban unit 2)

Table 3: Result of XRD interpretation(1-4)

The identified Minerals in bulk samples	Basalt	Volcaniclastics			Qatrani Sandstone
	North Ext. (N0)	Haddadin (Q4)	Rabwa (1)	Abu Roash (1B)	Rabwa (1B)
	Urban unit 3&4	Urban unit 2	Urban unit 2	Urban unit 1	Urban unit 2
Augite (Aug)	2.99Å(M)	-	-	-	-
Olivine (Ov)	2.50 Å(T)	-	-	-	-
Feldspars (Fd) (Labradorite)	3.19 Å(D)	3.19 Å(D)	3.22 Å(M)	3.21 Å(T)	3.21 Å(M)
Quartz (Qz)	3.35 Å(T)	-	3.38 Å(T)	3.34 Å(M)	3.34 Å(M)
Goethite (Gth)	-	-	-	2.45 Å(T)	2.45 Å(M)
Hematite (Hem)	-	2.68 Å(T)	-	-	-
Calcite (Cal)	3.01 Å(T)	3.00 Å(M)	3.04 Å(A)	3.03 Å(D)	2.99 Å(T)
Dolomite (Dol) (Ankerite)	2.89 Å(T)	2.89Aº(A)	2.90 Å(A)	2.89 Å(A)	2.89 Å(M)
Halite (Hal)	2.81 Å(T)	2.81 Å(M)	2.84 Å(T)	2.82 Å(M)	2.84 Å(T)
Gypsum (Gyp)	-	-	-	7.62 Å(T)	7.61 Å(T)
Anhydrite (An)	-	-	-	3.50 Å(T)	-
Smectite (Sm)	15.0 Å(T)	14.41 Å(M)	12.78 Å(T)	-	12.30 Å(T)
(-) Absent	**T = traces < 10%**	**M= moderate 10-20%**	**A= abundant 21-40 %**		**D= dominant > 40%**

Upon glycolation and heating, both shift to approximately 17 Å and ~10 Å, respectively.Several non-clay minerals such as calcite, quartz, and feldspars are the main components, with traces of halite and/or gypsum in some samples. Semi-quantitative (relative abundance) estimation of the identified clay minerals was done using the XRD charts, following the procedure of Shultz (1964) and Pierce and Siegel (1969).

4.3.2. Evaluation of geoengineering properties

The geoengineering characterization of selected bedrocks in urban units 1–4 is divided into two sections. The first evaluates the consolidated (compacted) volcanic rocks (Table 4), while the second focuses on the friable sedimentary rocks, such as the Qatrani sandstones (Table 5). The compacted volcaniclastic and basaltic rocks were tested for unit weight, unconfined compressive strength, Los Angeles abrasion, absorption, and degradation (Table 4). These properties vary due to differences in weathering, clay content and type, as revealed by petrographic thin sections and XRD analysis.
The integration of the geotechnical properties indicates that the fresh basalt (N0) out performs the highly altered basalt as well as the volcaniclastic bedrocks in all assessed properties (Table 4).

Table 4: Geoengineering properties of volcanic compacted bedrocks in the different urban units (1-4)

Location & Sample No.	Lithology	Unit weight gm/cm	CmS kg/cm^2	Los Angeles (Abr %)	Abs %	Deg %	Evaluation (Durability)
Rabwa (1A) (unit2)	Volcaniclastic	2.25	132	20.56	4.1	2.4	Medium durable
Haddadin (Q4) (unit2)	Volcaniclastic	2.33	150	20.61	10.8	5.6	Medium durable
N. Extension (N0) (units 3&4)	Fresh Basalt	2.55	184	17.85	3.3	1.8	Most durable
N. Extension (N1) (unit 3)	Weathered Amygdaloidal basalt	2.15	135	24.32	12.6	6.5	Least durable
Abu Roash (AR5) (unit 1)	Volcaniclastic	2.11	125	22.16	6.8	3.0	Medium durable

CmS = Compressive Strength, Abs = Abrasion, Abs = Absorption, Deg = Degradation

Table 5: Geoengineering properties of the friable bedrocks in the different urban units (2-4)

Location & Sample No.	Lithology	Mud content %	Water content %	CBR %	Proctor gm/cm^3	Classification (USCS)	Geotechnical evaluation
Rabwa (2A) (unit 2)	Green/White S S	12	0.90	12.0	1.92	SP	Medium hazardous soil
Rabwa (3) (unit 2)	Green S S	28.3	2.20	11.5	1.86	SM	Medium to high hazardous soil
Rabwa (5) (unit 2)	Ferruginous S S	36.4	0.20	13.0	2.02	SC	Medium hazardous soil
N.Extension (2) (units 3&4)	Brownish S S	13.3	1.23	13.4	1.90	SP	Medium hazardous soil
N.Extension (N0) (W) (units 3&4)	Friable weathered material of Basalt	63.6	6.10	16	1.95	CH	High hazardous soil

S S. = Qatrani Sandstones (formation), CBR = California Bearing Ratio, USCS = Unified Soil Classification System, SP = Poorly graded sand, SM = Muddy sand, SC = Clayey sand, CH = High plastic clay

Therefore, the fresh basalt is classified as a hard and highly durable rock, while other volcanic varieties are considered medium durable (Table 4). In contrast, the highly weathered volcanic rocks in Haddadin and Abu Roash contain significant amounts of expansive clays, reducing their durability and bearing capacity. As a result, they are the least durable and not suitable for foundation soils (Table 4). The geoengineering evaluation of the friable bedrocks started with classification using the Unified Soil Classification System (USCS). The percentage of fine materials (mud fraction) passing through the #200 sieve was determined. For the different types of Qatrani sandstones, mud content ranged from 12.0% to 36.4%, indicating a heterogeneous gradient and classifying them as medium to highly hazardous foundation soils (Table 5).

The California Bearing Ratio (CBR) of the sandstones ranges from 11.5% to 13.4% (Table 4), indicating low to medium swelling potential. In contrast, the friable basaltic weathered soils show high swelling potential, making them unsuitable as foundation soils. The modified Proctor and moisture (water) content values support these findings, indicating that sandstone bedrocks may have medium to high negative impacts on soil performance.

In conclusion, the geotechnical behavior of weathered volcanic and argillaceous sandstone bedrocks depend on the type and amount of clay minerals, their activity, and the associated moisture content. Significant swelling when wet or shrinkage when dry can severely damage foundations and buildings. Highly weathered volcanic bedrocks especially fractured volcaniclastic types in the North Extension, Haddadin, and Abu Roash urban units (Table 4) form highly plastic, compressible clays when exposed to subsoil water. In contrast, argillaceous clastic bedrocks like the Qatrani sandstone are heterogeneous and compressible but generally offer more favorable foundation conditions. However, over time and with increased land use and groundwater exposure, these conditions may deteriorate, leading to further structural damage.

4.4. An integrated risk assessment

The risk assessment of foundation site problems in the urban units (Table 2) and their bedrock outcrops (Figure 4) is complex due to various geological, geotechnical, and environmental factors (risk parameters) that influence potential negative impacts. Based on the spatial distribution of these parameters, two types of assessments are applied: geomorphological hazard assessment for the whole urban units, and geotechnical evaluation of the volcanic and clastic bedrocks in urban units 1, 2, 3, and 4 (Table 5). The semi-quantitative risk level is expressed as a numerical value from 1 to 10, where 1 indicates the least and 10 the highest negative impact. These values are grouped into low, medium, high, and very high risk levels, as shown in Tables 6 and 7.

4.4.1. Geomorphical risk assessment model

This model is proposed based on the spatial distribution of risk parameters, including geomorphological (landforms), geological (rock units and fracture intensity), and environmental (geohazards and urban expansion changes) factors across all urban units (Table 6).
Highly weathered basaltic soil is more hazardous for foundations compared to volcaniclastic rocks and clastic soils.

The spatial distribution of landforms (Figure 3), based on topographic elevation differences, shows two groups (sub-models) of urban units: a lowland group including U7, U8, U9, and U1, and a highland group including U1, U2, U3, U4, U5, U6, and U10. Each sub-model has its own external and internal characteristics, and therefore, distinct hazard specifications as shown in Table 5.

Uncontrolled urbanization in urban unit (11) and nearby low-lying areas of units (9) and (2) (Figure 4) has led to a gradual loss of fertile land due to urban expansion at the expense of traditionally cultivated areas. Additionally, these urban units are more vulnerable to negative impacts such as rising groundwater levels and potential soil liquefaction, mainly caused by poor drainage and sewage leakage near buildings and infrastructure.

Table 6: Geomorphic risk assessment of the urban units (Figure 4) as revealed from geomorphological, geological and environmental parameter

Risk Parameters (based on figs. 2,3,4&5)			**Risk levels in the urbans Units**										
			U 1	**U 2**	**U 3**	**U 4**	**U 5**	**U 6**	**U 7**	**U 8**	**U 9**	**U1 0**	**U1 1**
Geomorphological parameters Based on Fig. 3	**Landforms**	Platuea	(-)	(-)	-	6	7	7	(-)	(-)	(-)	(-)	(-)
		Hills	8	8	8	(-)	(-)	(-)	(-)	(-)	(-)	(-)	(-)
		Talus cover	(-)	4	4	-	-	3	3	(-)	(-)	(-)	(-)
		Wadi plaines	2	2	-	-	-	2	2	2	2	2	-
		Nile terraces	5	(-)	-	-	-	-	-	-	(-)	-	(-)
		Nile flood plain	(-)	(-)	-	-	-	(-)	(-)	(-)	(-)	-	8
		Structure dome	-	-	-	(-)	-	-	(-)	-	(-)	10	(-)
Geological parameters Based on Fig. 2	**Rock units & structures**	Qns	(-)	(-)	(-)	-	(-)	(-)	(-)	(-)	(-)	-	10
		Qnl	(-)	(-)	-	-	-	-	-	2	2	2	(-)
		Tpl	-	(-)	(-)	4	-	-	4	-	(-)	-	(-)
		Tplh	-	-	7	-	(-)	-	-	-	(-)	(-)	-
		Tmk	-	5	5	-	5	-	(-)	-	-	(-)	-
		Vb	9	9	9	9	2	3	-	-	-	-	-
		Toq	5	5	5	5	(-)	5	(-)	5	(-)	(-)	(-)
		Kuu	(-)	(-)	(-)	(-)	(-)	(-)	(-)	(-)	(-)	9	(-)
Environmental hazards potentiality	**Geohazards**	Fracture Intensity	6	8	9	3	8	8	2	1	3	10	2
		Slope instability	7	9	9	7	3	10	(-)	(-)	(-)	9	(-)
		Groundwater rise	2	-	(-)	(-)	(-)	(-)	(-)	(-)	(-)	3	9
	Urban expansion	2000	2	(-)	(-)	2	(-)	(-)	(-)	(-)	2	(-)	4
		2010	4	4	2	5	2	4	4	4	4	5	4
		2020	8	9	6	5	4	8	4	6	7	10	9
Average of risk levels			**6**	**6**	**7**	**6**	**4**	**5**	**3**	**3**	**3**	**6**	**7**

(-) = not represented

Risk categrois	**0-2**	**3-5**	**6-8**	**9-10**
	Low	**Medium**	**High**	**Very High**

As shown in Table 5, the low-lying urban areas within or near cultivated lands are classified as high-risk zones. Their risk levels are expected to increase when buildings are located at topographic levels close to or below the Nile water level. Moreover, aggressive land use and uncontrolled human activities further elevate the risk of negative impacts.

The urban units at relatively higher topographic levels (the high sub-model) are generally more vulnerable to land use hazards and are classified as high-risk areas (Table 5). Risk levels notably increase in steeply sloped escarpments and hills, especially in units U1, U2, U3, U4, U6, and U10. Buildings in these areas may be unsafe due to the potential for landslides and erosion caused by runoff water triggered during heavy rainfall, which may become more frequent with climate change.

4.4.2 Integration of geotechnical Risk assessment model

Based on the integration of geoengineering evaluation results (Tables 4 and 5) with the petrographic characteristics of the bedrock (Figures 6–8 and Table 3), a geotechnical risk assessment model has been developed, as presented in Table 7. The analysis shows that key petrographic and mineralogical factors influencing the risk level and category include vesicular and amygdaloidal textures, the type of secondary mineral compositions, and features linked to weathering and diagenesis. These factors and their effects are further explained in the following discussion.

1- Secondary minerals such as clay, iron oxides, carbonates, and evaporite minerals are found in different amounts and forms, often filling vesicles and amygdales. In some cases, they also replace primary minerals like feldspar and mafic components. A high concentration of these secondary minerals can greatly change the original hard and compact basaltic rocks, turning them into highly weathered and softer materials. This transformation raises the geotechnical risk of the rock mass when subjected to applied loads.
2- The highly calcareous vesicular and amygdaloidal basaltic and volcaniclastic bedrocks, with their high pore connectivity, allow subsoil water—often from different land use sources—to move easily through the rock. This increased moisture flow can raise capillary pressure, leading to partial disintegration and reduced bedrock stability, which increases geotechnical risk. Higher rock porosity is clearly linked to a greater tendency for disaggregation (Espert *et al.,* 1981).
3- Carbonate minerals in the highly calcareous volcaniclastic rocks—such as those found in Abu Roash (Unit 1) and Rabwa (Unit 2)—are prone to alteration through partial dissolution by subsoil water. This process can create irregular voids and small cavities, leading to the weakening and degradation of the bedrock structure. It is widely accepted that the dissolution of carbonate and clay components in bedrock is mainly caused by circulating meteoric water within active weathering zones (Longman, 1980).
4- The argillaceous sandstone, basaltic volcaniclastic rocks, and highly altered basalt bedrocks contain notable amounts of Na-smectite and Ca-smectite (montmorillonite), as shown in Table 3. These clay minerals have expansive and contractive behavior that strongly affects the physical properties of the host rocks. Smectites, known for their high swelling potential, can significantly reduce the stability and mechanical performance of the bedrock, especially when moisture conditions change (Bell and Maud, 1995; Houben and Guillaud, 1994; Nelson and Miller, 1997; Moore and Reynolds, 1997; Meisina, 2004).

Smectite can swell to several times its dry volume depending on water availability. As a result, repeated swelling and shrinkage during alternating wet and dry seasons—caused by changes in humidity and temperature—can significantly contribute to the disintegration or severe deterioration of the bedrock. This cyclical expansion and contraction generates internal stress, gradually weakening the rock structure over time.

5- Evaporites such as halite, gypsum, and other water-soluble salts occur diagenetically within the basalt and basaltic volcaniclastic bedrocks in the study area (Table 3). The presence of these soluble salts is a major factor contributing to bedrock damage. Salt weathering and the growth of salt crystals within pores and microfractures can cause significant deterioration, as documented by several researchers (e.g., Bongrani and Fanfoni, 1995; Goudie and Viles, 1997).

Evaporite minerals such as halite, gypsum, and other water-soluble salts occur diagenetically within the basalt and basaltic volcaniclastic bedrocks of the study area (Table 3). These salts are a key factor in bedrock deterioration. Salt weathering, especially from crystallization and growth within pores and microfractures, can create strong internal pressure, causing mechanical breakdown and structural damage. The harmful effects of salt crystallization on rock integrity have been well documented by several researchers (e.g., Bongrani and Fanfoni, 1995; Goudie and Viles, 1997).

The clayey bedrocks such as the highly weathered volcaniclastic rocks contain large amounts of expansive clays and are characterized by low bearing capacity. These materials fall under high-risk categories in geotechnical assessments. When expansive clays interact with infiltrating water from green areas or other land use sources, they can cause ground instability and differential settlement. This may lead to structural damage, including cracking and deformation, especially in the highly altered volcaniclastic bedrocks during heavy rainfall or occasional earthquakes. In areas with intense fracturing, the risk level increases further and is classified as high-risk, as shown in Table 7.

Table 7 : Integrated geotechnical risk assessment of the compacted and friable bedrocks based on petrographic characteristics and Tables 4 & 5

Type	Location & Sample No	Integrated petrographic controling parameters	Risk level and category
Compacted bedrocks	Rabwa urban unit2 (1A)	Volcaniclastic, calcareous,glassy,small amygdales with little secondary material and clays	(4) Medium risk
	El-Haddadin urban unit 2 (Q4)	Volcaniclastic, highly calcareous, large amygdales and vesicles with considerable amount of expansive clay and halite	(7) High risk
	N. Ex., urban units 3&4 (N0)	Fresh basalt, with slightly altered feldspar and olivine with traces of smectite	(3) Medium risk
	N.Ex., urban unit 3&4 (N1)	Highly weathered amygdaloidal basalt in contact with clayey sandstone, rich in secondary materials and muddy layers.	(8) High risk
	Abu Roash, urban unit1 (AR5)	Volcaniclastic, scoracious glassy basaltic rock with altered feldspars and expansive clays	(5) Medium risk
Friable bedrock	Rabwa, urban unit 2 (2A)	Highly calcarous, clayey sandstone with altered feldspar, carbonates, and evaporite cement materials	(3) High risk
	Rabwa, urban unit 2 (3)	Highly argillaceous sandstone with microfractures, clay and silica cement	(6) High risk
	Rabwa urban unit 2, (5)	Ferruginous sandstone, poorly sorted with considerable mud content and iron cement materials	(5) Medium risk
	N. Ex., urban units 3&4 (2)	Poorly graded iron stained clayey sandstone with fine gravels in contact with heterogenous volcaniclastic	(4) Medium risk.
	N. Ex., urban unit 3&4 (N0w)	Friable weathered material of basalt, rich in minerals and small basaltic fragments	(8) High risk

Genesis of the volcaniclastic rocks:

5. Conclusion and Recommendation

In desert regions such as the October–Abu Roash stretch, where buildings are founded on heterogeneous volcaniclastic bedrocks containing expansive clay, weathered carbonate and disolved secondary mineral components, lithomorphic and geoengineering analyses play a pivotal role in geotechnical evaluation and in predicting structural behavior under loading conditions and intensive urban landscape changes. The study area is potentially threatened by natural environmental exogenic hazards, including construction on steep slopes of unstable escarpments and development within the cultivated Nile floodplain. The bedrock lithotopes are susceptible to weathering and further alteration particularly within the land use and climate changes.

Although the volcaniclastic bedrocks generally exhibit acceptable bearing capacity and high durability, their weathered, carbonate and clay-rich varieties are highly sensitive to exposure to subsurface water from any source. This sensitivity is primarily due to the swelling and shrinking

behavior of the expansive clay components and secondary porosity formation within the bedrocks in response to moisture variations. Such alternating volumetric changes can lead to significant and potentially devastating damage to foundation conditions.

An integrated geomorphic and geotechnical risk assessment was carried out based on the identified geological, geomorphological, petrographical, clay mineralogical, and geoengineering risk parameters. This assessment serves as a crucial guide for selecting suitable sites for future urban expansion.

Based on the current geotechnical evaluation, the following recommendations are proposed to mitigate the negative impacts and challenges associated with litho- heterogenous and expansive clay-rich foundation bedrocks.

The primary interaction between potential subsurface water infiltration and expansive clay-rich volcaniclastic foundation bedrocks should be mitigated by minimizing sources of excess water—such as reducing irrigation in green areas within existing urban developments.

For selecting potential sites for future urban expansion, it is generally advisable to remove the shallow, highly weathered, clay-rich volcaniclastic foundation bedrocks to a suitable depth. Backfilling should then be performed using a well-graded mixture of sand and fine gravel, containing only a small percentage of fine silt. Finally, the replaced soils must be properly compacted to achieve the required maximum dry density and optimum moisture content, ensuring their suitability for foundation purposes.

References

Aashto, T. 2002. Standard method of test for resistance to degradation of small-size coarse aggregate by abrasion and impact in the Los Angeles machine. American Association of State Highway and Transportation Officials.

Abdel khalek, M.L., et al.,1989. Structural history of Abu Roash stretch, Western Desert, Egypt. Journal African Earth Sciences 9: 435-443.

Arnous, M.O., H.A. Aboulela, , and D.R. Green, 2011. Geo-environmental hazards assessment of the north western Gulf of Suez, Egypt. Journal of Coastal Conservation, 15: 37-50.

ASTM D1556-07; 2007. Standard Test Method for Density and Unit Weight of Soil in Place by the Sand-Cone Method. American Society for Testing and Materials: West Conshohocken, PA, USA.

ASTM-D1883, 2021. Standard test methods for California Bearing Ratio (CBR) of laboratory-compacted soil, ASTM International, West Conshohocken, PA.

ASTM-D2216, 2019. Standard test methods for laboratory determination of water (moisture) content of soil and rock by mass, ASTM International, West Conshohochen, PA.

ASTM-D570, 1998. Standard Test Method for Water Absorption of Plastics, ASTM International, West Conshohocken,PA.

Bell, F.G., and R.R. Maud, 1995. Expansive clays and construction, especially of low-rise structures: a viewpoint from Natal, South Africa. Environmental & Engineering Geoscience, 1(1): 41-59.

Bongrani, L., and G. Fanfoni, 1995. Advanced restoration techniques against the effects of soluble salts in the stone of the Egyptian monuments. In Proceedings of the Egyptian-Italian seminar on geosciences and archaeology in the mediterranean countries (253-260).

Conoco, Map, Egypt, Geological map of Egypt. Scale: 1:500,000 (1987).

Embabi, N.S., 2004. The Geomorphology of Egypt, Egyptian geographical society.

Goudie, A.S., H.A. Viles, , and A.G. Parker, 1997. Monitoring of rapid salt weathering in the central Namib Desert using limestone blocks. Journal of Arid Environments, 37(4): 581-598.

Houben, H. and H. Guillaud, 1994. Earth Construction- A Comprehensive Guide. Intermediate Technology, London. 1994.

Hussien, H.A., *et al.,* 1987. Areportonthe treatment, rejuvenation, operation and studying of the Nadi El Remaia water field, 6th of October City, 325 (in Arabic).

Longman, M.W. 1980. Carbonate diagenetic textures from nearsurface diagenetic environments. AAPG bulletin, 64(4): 461-487.

Meisina, C. 2004. Swelling-shrinking properties of weathered clayey soils associated with shallow landslides. Quarterly journal of engineering geology and hydrogeology, 37(2): 77-94.

Moore, D.M., R.C. Reynolds, 1997. X-Ray Diffraction and the identification and analysis of clay minerals. Oxford University Press, pp:378.

Nelson, J.D., and D.G. Miller, 1997. Expansive Soil: problems and practice in foundation and pavement engineering. John Wiley & Sons, New York, 288.

Pierce, J.W., and F.R. Siegel, 1969. Quantification in clay mineral studies of sediments and sedimentary rocks. J. Sed. Petrol. 39: 187-193.

Shallaly, N.A., 1998. The Tertiary basaltic rocks of Gabal Qatrani- the 6th October city area, GAW4, Inter-Conf.Geo. the Arab world.

Shultz, L.G., 1964. Quantitative interpretation of mineralogical composition from X-ray and chemical data from the Pierre Shale. U S. Geol. Surv., 26:175-207.

Youssef, A.M., and N.H. Maerz, 2013. Overview of some geological hazards in the Saudi Arabia. Environmental Earth Sciences, 70: 3115-3130.